

Award Number: W81XWH-18-1-0101

TITLE: Innovative Ultrasonic Methods for the Diagnosis and Monitoring of Pulmonary Fibrosis

PRINCIPAL INVESTIGATOR: Dr. Marie Muller

CONTRACTING ORGANIZATION: North Carolina State University,  
Raleigh, NC, 27695

REPORT DATE: May 2020

TYPE OF REPORT: Annual

PREPARED FOR: U.S. Army Medical Research and Materiel Command  
Fort Detrick, Maryland 21702-5012

DISTRIBUTION STATEMENT:

Approved for public release; distribution unlimited

The views, opinions and/or findings contained in this report are those of the author(s) and should not be construed as an official Department of the Army position, policy or decision unless so

# REPORT DOCUMENTATION PAGE

Form Approved  
OMB No. 0704-0188

Public reporting burden for this collection of information is estimated to average 1 hour per response, including the time for reviewing instructions, searching existing data sources, gathering and maintaining the data needed, and completing and reviewing this collection of information. Send comments regarding this burden estimate or any other aspect of this collection of information, including suggestions for reducing this burden to Department of Defense, Washington Headquarters Services, Directorate for Information Operations and Reports (0704-0188), 1215 Jefferson Davis Highway, Suite 1204, Arlington, VA 22202-4302. Respondents should be aware that notwithstanding any other provision of law, no person shall be subject to any penalty for failing to comply with a collection of information if it does not display a currently valid OMB control number. **PLEASE DO NOT RETURN YOUR FORM TO THE ABOVE ADDRESS.**

<b>1. REPORT DATE</b> MAY 2020	<b>2. REPORT TYPE</b> Annual	<b>3. DATES COVERED</b> 15APR2019 - 14APR2020
<b>4. TITLE AND SUBTITLE</b>  Innovative Ultrasonic Methods for the Diagnosis and Monitoring of Pulmonary Fibrosis		<b>5a. CONTRACT NUMBER</b>
		<b>5b. GRANT NUMBER</b> W81XWH-18-1-0101
		<b>5c. PROGRAM ELEMENT NUMBER</b>
<b>6. AUTHOR(S)</b>  Marie Muller Dr. Thomas Egan         E-Mail:mmuller2@ncsu.edu		<b>5d. PROJECT NUMBER</b>
		<b>5e. TASK NUMBER</b>
		<b>5f. WORK UNIT NUMBER</b>
<b>7. PERFORMING ORGANIZATION NAME(S) AND ADDRESS(ES)</b>  North Carolina State University Raleigh, NC, 27695		<b>8. PERFORMING ORGANIZATION REPORT NUMBER</b>
<b>9. SPONSORING / MONITORING AGENCY NAME(S) AND ADDRESS(ES)</b>  U.S. Army Medical Research and Materiel Command FORT DETRICK, MARYLAND 21702-5012		<b>10. SPONSOR/MONITOR'S ACRONYM(S)</b>

## 12. DISTRIBUTION / AVAILABILITY STATEMENT

Approved for Public Release; Distribution Unlimited

## 13. SUPPLEMENTARY NOTES

## 14. ABSTRACT

Idiopathic pulmonary fibrosis (IPF), affecting 200,000 patients in the U.S leads to changes in the micro-architecture of the parenchyma, such as thickening of the alveolar walls. This study investigates the use of ultrasound to detect these changes, by exploiting ultrasound multiple scattering by the air-filled alveoli. In a highly scattering media such as the parenchyma, ultrasound propagation follows a diffusion process which can be characterized using the Diffusion Constant. We hypothesized that in a fibrotic lung, the thickening of the alveolar wall reduces the amount of air, minimizing the scattering events and changing the scattering pattern.

Pulmonary fibrosis was created in Sprague-Dawley rats by bleomycin inhalation. The animals were studied in groups of n=6 2, 3, and 4 weeks after bleomycin administration, allowing to evaluate a range of severity of pulmonary fibrosis. The Diffusion Constant was measured using a linear array ultrasound transducer *in vivo*. The rats were then euthanized. Computed Tomography and histology evaluation were performed to estimate the degree of fibrosis created. Significant differences ( $p < 0.05$ ) in the D values between control and fibrotic rats. Correlations of D with the CT and histology data were observed. This suggest the potential of this method for diagnosis and monitoring of IPF.

## 15. SUBJECT TERMS

Ultrasound, pulmonary fibrosis, staging, monitoring, multiple scattering, diffusion

## 16. SECURITY CLASSIFICATION OF:

17. LIMITATION  
OF ABSTRACT18. NUMBER  
OF PAGES

## 19a. NAME OF RESPONSIBLE PERSON

## a. REPORT

## b. ABSTRACT

## c. THIS PAGE

USAMRDC

19b. TELEPHONE NUMBER (include area  
code)

Unclassified

Unclassified

Unclassified

Unclassified

19

## Table of Contents

**16 Pages**

<b>1. Introduction.....</b>	<b>2</b>
<b>2. Keywords.....</b>	<b>3</b>
<b>3. Accomplishments.....</b>	<b>3</b>
<b>4. Impact.....</b>	<b>11</b>
<b>5. Changes/Problems.....</b>	<b>12</b>
<b>6. Products, Inventions, Patent Applications, and/or Licenses.....</b>	<b>12</b>
<b>7. Participants &amp; Other Collaborating Organizations.....</b>	<b>12</b>
<b>8. Special Reporting Requirements.....</b>	<b>13</b>
<b>9. Appendices.....</b>	<b>13</b>
<b>10. References.....</b>	<b>13</b>

## 1. Introduction

Pulmonary fibrosis is a progressive, fatal, inflammatory and fibro-proliferative lung disease. The main histopathological features of pulmonary fibrosis, best seen at low magnification, is a heterogeneous appearance with areas of sub-pleural and para-septal fibrosis and honeycombing (ie, cystic fibrotic airspaces often filled by mucin and variable numbers of inflammatory cells) alternating with areas of less affected or normal parenchyma, heterogeneously distributed. In pulmonary fibrosis, interstitial lobular septa are thickened by collagen tissue accumulation, forming patchy scars and leading to chronic inflammation(Katzenstein and Myers 1998).

Conventional chest radiography and high-resolution computer tomography (HRCT) are the most common techniques to diagnose pulmonary fibrosis as well as assess treatment efficiency. High-resolution CT (HRCT) of the chest has been found to be a sensitive and reproducible method to assess the extent and pattern of pulmonary fibrosis(Luna Gargani et al. 2009; Launay et al. 2006; Desai et al. 2007). However, they are associated with high radiation, inflated costs and very low portability. All these disadvantages represent a particular challenge in the context of monitoring, where repeated evaluations have to be made for a given patient.

Lung ultrasound (LUS) is a non-invasive, cheap and portable modality. LUS has multiple uses, both in diagnosis as well as intervention. A number of studies show that LUS, as a consequence of its advantages over radiography and HRCT (no radiation exposure, cost effective and high portability) can play the primary role in diagnosis and monitoring of fibrosis (Sayed et al. 2016). However the presence of air-filled alveoli has long been considered a major obstacle to ultrasound imaging, leading to numerous artefacts. Lately, these artifacts have been recognized to have some diagnostic potential. The conventional approach of lung ultrasound is based on the identification of standardized signs(Lichtenstein 2016; Soldati and Sher 2009). Pulmonary fibrosis is associated with the presence of Ultrasound Lung Comets (ULCs), an echographic artifact detectable with chest sonography(Luna Gargani et al. 2009; Picano et al. 2006). The images exhibit multiple comet tails fanning out from the lung surface as shown in Figure 1(Luna Gargani et al. 2009; Jambrik et al. 2004). In pulmonary fibrosis, ULCs are generated by the reflection of the ultrasound beam from thickened sub-pleural interlobular septa(Reiβig and Kroegel 2003). However, these artifacts are highly qualitative, and reading and interpreting these signs is subjective and operator-dependent. ***They're not observed consistently, and, being qualitative, they don't allow for monitoring or staging.***

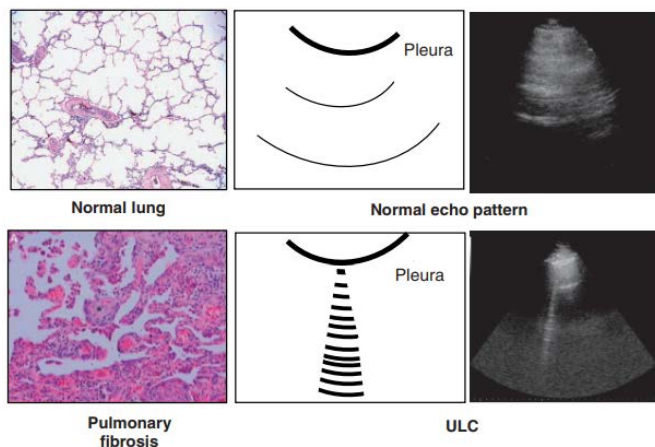
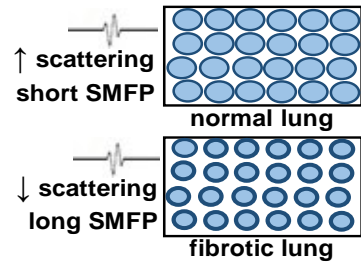


Figure 1: Reflections of the ultrasound beam by thickened interlobular septa give rise to ULCs.

***The quantitative tissue characterization of the lungs has remained a challenge using acoustic and ultrasound techniques.*** The presence of air sacs make the lung a highly diffusive, aberrating and scattering medium. The diffusive nature of the lung destroys the linear relationship between propagation time and propagation distance thereby making imaging of the parenchyma impossible. We proposed to leverage these large amounts of scattering.

The proposed approach is based on the following hypothesis: because pulmonary fibrosis is responsible for changes in the micro-architecture of the parenchyma - thickening of the alveolar walls, which reduces compliance and elasticity – it can be hypothesized that multiple scattering of ultrasound waves can be used to detect and quantify these changes. *In the fibrotic lung, alveolar wall thickening and reduced amount of air will lead to a reduced number of scattering events, which will be detected and quantified by this new approach.* The approach relies on the measurement of the scattering mean free path (SMFP), which is the mean distance between scattering events (Derode et al, PRL, 2003). In the healthy, normal lung, the millions of air-filled alveoli are responsible for frequent scattering events, leading to short SMFPs. *In contrast, in pulmonary fibrosis, due to reduced volume of air, and increased volume of tissue, less scattering should be observed. Therefore the SMFP is expected to be significantly longer in fibrotic lungs than in normal lungs (Fig.2).*



**Fig.2.** Blue = air-filled alveoli. **Top:** ultrasound wave into normal lung experiences multiple scatters, so SMFP is short. **Bottom:** Fibrotic lungs have smaller alveoli, thicker alveolar walls, and more tissue between alveoli, so distance between scatters is longer.

Because of the principle of the SMFP measurement, it is expected that other pathologies, such as pulmonary edema, will also lead to increased values of SMFP compared to healthy lungs. In order to make sure that the method developed here can provide a univocal diagnosis and quantification of fibrosis, an additional parameter was evaluated: the Backscatter Frequency Shift (BFS). Indeed, it is expected that the frequency content of ultrasonic waves propagating through the parenchyma will be modified by the presence of fibrotic tissue. A downshift of the frequency is expected in the fibrotic lung, due to a higher absorption by the fibrotic tissue. The frequency downshift is not expected to be as high in the edematous lung, because absorption of high frequencies through water (edematous lung) is expected to be less than through air (normal lung) or fibrotic tissue (fibrotic lung). We expect the SMFP to discriminate fibrotic from healthy lungs, and the BFS to discriminate pulmonary edema, or other lung disease leading to increased lung water, from pulmonary fibrosis.

## 2. Keywords

Ultrasound, pulmonary fibrosis, staging, monitoring, multiple scattering, diffusion

## 3. Accomplishments

### 3.1 Major Goals

We had two major goals for this project.

The first goal was to create various levels of fibrosis severity in a rodent model of pulmonary fibrosis. By instilling bleomycin into the airway of male and female Sprague-Dawley rats, and acquiring ultrasound, CT and histology data 2, 3 and 4 weeks after instillation.

The second goal was to determine whether the SMFP could be used to quantify severity of pulmonary fibrosis.

### **3.2 Accomplishments under these goals**

#### **Bleomycin Rat Model**

Pulmonary fibrosis was created in Sprague-Dawley rats by instilling bleomycin into the airway. After sedation, rats were intubated with a 12-gauge catheter. Bleomycin 2mg/kg, dissolved in 100  $\mu$ l sterile PBS, was administered into the trachea. The rat was extubated and allowed to recover. The bleomycin causes development of pulmonary fibrosis within 2-3 weeks (Xu et al. 2006; Rojas et al. 2005; Moeller et al. 2008). Rats were studied in groups of n=6 (3 male and 3 female) 2, 3, and 4 weeks after bleomycin administration, to create a range of severity of pulmonary fibrosis for assessment (Chaudhary, Schnapp, and Park 2006). Six rats (3 male, 3 female) who receive no treatment served as controls.

#### **Rat model of pulmonary edema**

Pulmonary edema was created in 6 more animals by using a lung hilar clamp model creating ischemia-reperfusion injury. The rats were anesthetized with an intraperitoneal (ip) injection of ketamine (100 mg/kg) and xylazine (10 mg/kg), and intubated via tracheotomy through a cervical incision. Rats were ventilated with FiO<sub>2</sub> 1.0, tidal volume (TV) of 0.75 ml/100 gm body weight, rate 70/min, 3 cm H<sub>2</sub>O PEEP. Anesthesia was maintained with isoflurane (0.5 - 4 %). Anesthesia depth was judged by toe pinch every 30 min. The jugular vein was cannulated for infusion of endotoxin-free albumin 2.5% in Ringer's lactate with 2% glucose buffered to pH 7.0 at 2 ml/hr by syringe pump to maintain hydration. Animal temperature was monitored with a rectal probe and maintained at 37°C on a heating pad intermittently turned on and off. The anesthetized rat was placed in the right lateral decubitus position, and a left lateral thoracotomy was performed in the 4th intercostal space. The left pulmonary hilum was dissected free. A small laparotomy incision exposes the liver. 600 U of heparin was injected intrahepatically. After 5 minutes, the left lung hilum was clamped with a clip for 60 minutes to render the left lung ischemic. Then the clip is removed and the left lung reperfused for 30 minutes.

#### **Animal Preparation for Ultrasound**

A total of 30 Sprague Dawley rats (6 controls, 6 edematous, 6 2 weeks after bleomycin instillation, 6 3 weeks after bleomycin instillation, 6 4 weeks after bleomycin instillation, for a total of 15 male and 15 female) were used in this study (349 $\pm$ 91.76 gms). After sedation, a tracheotomy was performed. Rats were ventilated with a Harvard rodent ventilator. Anesthesia was maintained with titrated isoflurane. A sternotomy was performed, both pleural spaces were opened, and the sternal edges spread maximally to expose both lungs. This had to be done because in the rat, the intercostal space is not large enough to fit an ultrasound probe. In human applications, we envision a completely non-invasive procedure, where the probe will be placed at multiple intercostal spaces. In rats, the incision was extended inferiorly into the abdomen to expose the liver. Heparin was administered intrahepatically to prevent clotting after the lungs were removed. For the ultrasound measurements, ultrasound coupling gel was applied directly onto each lung. Ultrasound measurements were taken in rat lungs *in vivo* (described below). After the ultrasound data was collected, the rat was euthanized by cardiectomy under anesthesia. The trachea was

clamped at end-inspiration. The heart-lung block was excised. The heart-lung block was immersed in cold phosphate buffered saline (PBS) for an ex-vivo CT scan (described below). Following the CT scan, the heart-lung block underwent inflation fixation for histologic interpretation (described below).

## **Data Acquisition methodology**

### **Scattering Mean Free Path**

All the in-vivo experiments were conducted with a 128 element Linear Array Transducer (Verasonics L11-4v ) connected to a Verasonics Vantage ultrasound scanner. For each animal, 10 ultrasound data sets were acquired to assess repeatability and reproducibility. The transducer was placed on the exposed lung using an approximately 2 mm layer of coupling gel. All of the elements of the array were fired one by one, transmitting a 2 cycle pulse with a central frequency of 7.8 MHz (300kPa in water) into the medium. For each transmit, the backscattered signals were collected on all 128 elements of the array. This gave us access to the spatial spread of the transient pressure field. The sampling frequency of the data acquired was 62.5 MHz and the total data acquisition time was set to 40  $\mu$ s. This enabled the acquisition of a 128 by 128 by 2500 impulse response matrix (IRM)  $\mathbf{H}(\mathbf{t})$  whose individual elements  $h_{ij}(t)$  are the  $N^2$  impulse responses of the medium.  $\mathbf{H}(\mathbf{t})$  was then processed using the methodology earlier described by Tourin et al and Aubry et al.(Aubry and Derode 2007; Tourin et al. 2000). For simplicity purpose, the origin time ( $t=0$ ) was set to the arrival of the first backscattered wave for every single receiving transducer. The IRM's reciprocity feature is exploited to generate the anti IRM represented by  $\mathbf{H}^A(\mathbf{t})$ . This is done using a simple matrix manipulation as shown.

- for  $i > j$ ,  $h_{ij}^A = -h_{ij}$ ;
- for  $i = j$ ,  $h_{ii} = 0$ ;
- for  $i < j$ ,  $h_{ij}^A = h_{ij}$ ;

$\mathbf{H}(\mathbf{t})$  and  $\mathbf{H}^A(\mathbf{t})$  were then processed to obtain D from the incoherent intensity. Analytically, the incoherent intensity can be represented as

$$I_{inc}(X, T) = I(T) \exp\left(-\frac{X^2}{4DT}\right), \text{(Eq.1)}$$

Where X represents the distance between emitter and receiver. The Diffusion constant D is an indicator of the diffusivity of the multiple scattering medium. Equation (1) clearly establishes that D can be retrieved by plotting the incoherent intensity as a function of X and T. The incoherent intensity is averaged over all emitter receiver couples separated by the same distance. At each time window, the backscattered incoherent intensity  $I_{inc}$  is fitted with a Gaussian curve and the variance of the Gaussian fit represents the dynamic growth of the diffusive halo given by ( $W^2(T) = 2DT$ ). Once D is extracted, the transport mean free path  $L^*$  is evaluated based on equation 2.

$$D = \frac{V_E \times L^*}{3} \quad \text{(Eq.2)}$$

### **Backscatter Frequency Shift**

In order to evaluate the Backscattered Frequency shift (BFS), plane waves with a central frequency of 6.5 MHz were transmitted through the parenchyma using all 128 elements and the

Radio Frequency (RF) data was recorded on all receivers. The spectral information was estimated from the RF data. Each RF line was split into 50% overlapping time windows and the power spectra of each line was estimated using a Hanning Window. Once the power spectral data of each line was obtained, the decay rate at which the power of the highest frequency within the -16dB bandwidth was calculated. This decay was then averaged over all 128 lines and linearly fitted. The slope of this linear fit was evaluated to be the BFS.

### **High Resolution CT Scanning and Scoring**

In order to optimize the resolution, *ex-vivo* high resolution CT scans were performed rather than imaging lungs in the alive, sedated, breathing animal. A high resolution preclinical CT system (CT 120, TriFoil Imaging, Inc. Chatsworth, CA) was used to acquire micro-CT images on lung specimens. The entire lung was removed from deceased rats, inflated, and closed at the airway. Images were immediately taken after lung collection with x-ray energy of 100 kVp, current of 50mA, 100 ms of exposure time, and 2x2 binning. Images were reconstructed using Feldkamp reconstruction algorithm to create isotropical CT images with nominal resolution of 50  $\mu$ m. Final images were converted to DICOM format with Hounsfield unit (HU). Before imaging, the lung block was inflated manually with air by syringe to a volume that visually approximates the volume of the lung block at end-inspiration when it was removed. It should be noted that compliance will be different for each lung block, depending on the amount of fibrosis. Inflation at the imaging facility to a particular inspiratory pressure or precise volume is not possible. Volume will change because lung cells remain viable for hours after circulatory arrest, so oxygen consumption is ongoing. With a respiratory quotient of 0.8 (CO<sub>2</sub> production to O<sub>2</sub> consumption), the volume of air in the lung block will diminish with time, so inflation was required. Imaging were taken within 10 min of inflation for all the specimens.

Severity of lung fibrosis was scored blindly from 0-4 based on visual assessment on fibrotic tissue volume based on the Ashcroft scale, with 0 being no fibrosis, 1 being small local fibrosis affecting less than 15% lung volume, 2 being local medium fibrosis affecting up to quarter of lung volume, 3 being large amounts of fibrotic tissue affecting up to 50% lung volume, 4 being diffusive fibrosis affecting multiple lung lobes with more than 50% lung volume.

### **Histology and Scoring**

After each CT scan, the lung blocks were subjected to inflation-fixation. Lung blocks were submerged in paraformaldehyde for 24-48 hours, then washed and stored in 70% ethanol. A paraffin section of lung, stained either by Hematoxylin and Eosin (5 micron sections stained with H&E) or by a trichrome method, was systematically scanned using a microscope with a 10x magnification. Each successive field was individually assessed for severity of interstitial fibrosis. Severity of lung fibrosis was studied on the Ashcroft scale (0-8 scaling) and then converted to a 0-4 scale (Robbe et al. 2015; Hübner et al. 2008; Ashcroft, Simpson, and Timbrell 1988). After examining the whole section, the mean score of all the fields were taken as the fibrosis histology score for the section. A veterinary lung pathologist provided a qualitative score based on the alveolar wall thickness in a masked manner.

## Data Analysis and statistical methods

The diffusion constant was calculated from IRM acquisitions. Differences between  $L^*$  values obtained from control and fibrotic lungs were tested using the Kruskal–Wallis test with Dunn’s post-test (data was not normally distributed, so non-parametric analysis was chosen). All data are presented as mean  $\pm$  standard deviation. All data are presented as mean  $\pm$  standard deviation. Statistical significance was set a priori at  $p < 0.05$  and is graphically depicted on all figures as (\*) for  $p < 0.05$ , (\*\*) for  $p < 0.01$  and (\*\*\*) for  $p < 0.001$ . NS to denote non-statistically significant comparisons. Statistics were performed in MatLab 2018a. All of our quantitative results will be transmitted to a statistician, from the Dept. of Statistics at NC State university, who will perform a more thorough statistical study.

Due to the very low penetration in control rat lungs, only the first portion of the variance plots as a function of time were selected to calculate the Diffusion Constant. This was automated using the *findchangepts* command in MatLab. For a trend to qualify, The  $R^2$  of the trend should be greater than 0.4. Data sets were also rejected for post processing if no multiple scattering was exhibited. This can be attributed to the lung operating at full volume capacity. Thanks to this observation, we now understand that it is advisable to acquire data in the exhaling cycle to ensure penetration and observe multiple scattering.

## Results

Shown in Figure 3 are examples of the variance plots obtained for a control lung and a 3Wk fibrotic lung.

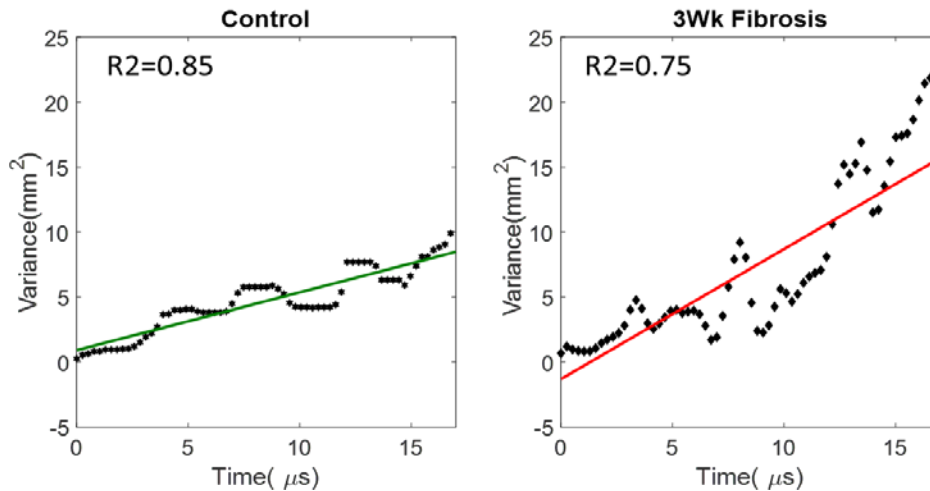


Figure 3: Variance growth for in-vivo rodent data

For the 3Wk fibrosis case, the variance increases more rapidly than for the control case. This can be attributed to thickened alveolar interstitial spaces which effectively increase the distance between air scatterers, allowing the wave to diffuse more freely. In the case of the control rat lungs, the growth of the diffusive halo is highly restricted due to the large air volume present in the lungs.

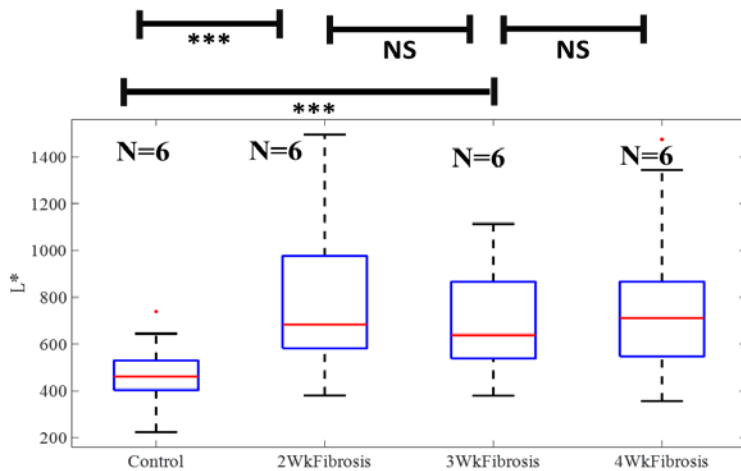


Figure 4: L\* Values for 4 groups of rats in vivo. \*\*\*: significant difference. NS: non significant

Shown in Figure 4 are the distributions of L\* values obtained in control and fibrotic lungs 2, 3, and 4 weeks after bleomycin inhalation. It can be seen that we are able to differentiate between control and fibrosis (2Wk, 3Wk and 4Wk) with high statistical significance. The L\* for control, 2Wk fibrosis, 3 Wk fibrosis and 4 Wk fibrosis were found to be  $466 \pm 109 \mu\text{m}$ ,  $773 \pm 304 \mu\text{m}$ ,  $690 \pm 191 \mu\text{m}$  and  $729 \pm 245 \mu\text{m}$  respectively. The error bars can be attributed to two major phenomena.

First, these readings are in-vivo and our attempt to acquire at the exhaling stage based on visual observation could be a potential source of error. Secondly, the lungs (size=3 cm) were much smaller than the transducer (3.8 cm). This could potentially allow signals from nearby regions to creep in and artificially increase the L\*. This could result in an over prediction of L\* which would not represent a challenge in larger animal models or in humans.

It can also be noted that although significantly different values of L\* were found for control rats and rats exposed to bleomycin, no significant differences can be observed between the supposedly different stages of fibrosis (ie 2, 3 and 4 weeks after bleomycin).

In order to validate the ultrasound results, it is important to analyze the CT and histology scores. Shown in Figure 5 and Figure 6 examples of CT and histology images, which were used to estimate fibrosis severity scores.

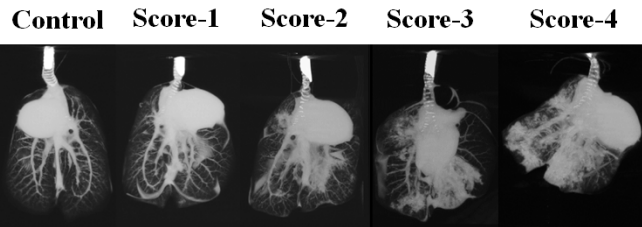


Figure 5: CT Images and their corresponding severity scores

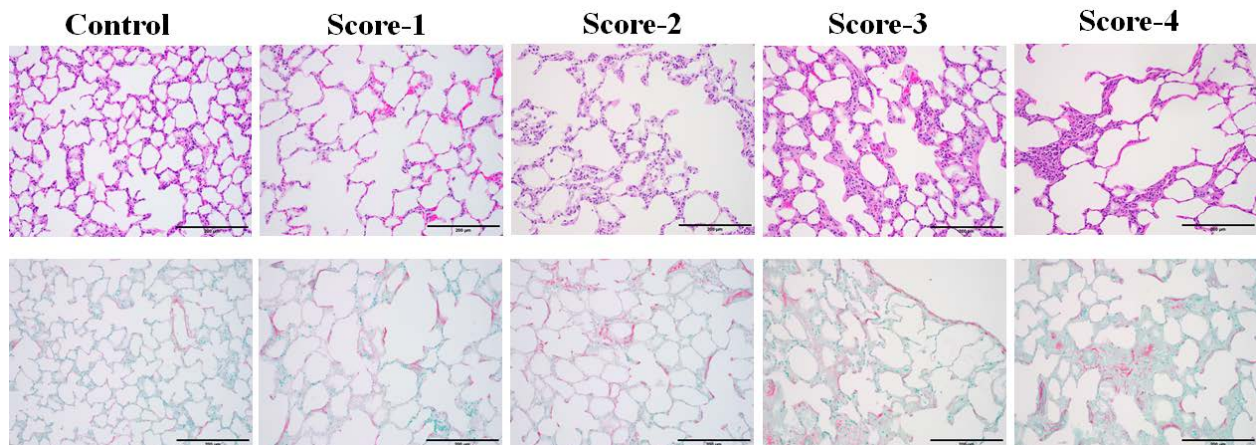


Figure 6: Histology images and their corresponding scores. Top: H&E staining. Bottom: Trichrome method

As fibrosis progresses, the tissue starts thickening which can be observed in histology images as well as the CT images. At score 4 of CT, we see higher shades of gray which reflect thickened septa. This is corroborated by histology images. Shown in Figure 7 and Figure 8 are the distributions for the fibrosis severity score for control, 2, 3 and 4 Wk fibrosis obtained from CT and histology images.

It can be seen from Figures 7 and 8 that maximum amount of fibrosis (as measured by CT and histology respectively) occurs after 2 weeks of bleomycin treatment and after which, fibrosis starts subsiding and is minimum at 4 weeks. On the other hand, histology also supports a similar claim wherein fibrosis does peak after 2 weeks of bleomycin administration. Shown in Table 1 are the average severity scores obtained from histology and CT.

Rat Type	CT Score	Histology Score
Control	0	0
2Wk	2.8	2.6
3Wk	2.2	1.8
4Wk	2	2.25

Table 1: Average severity scores

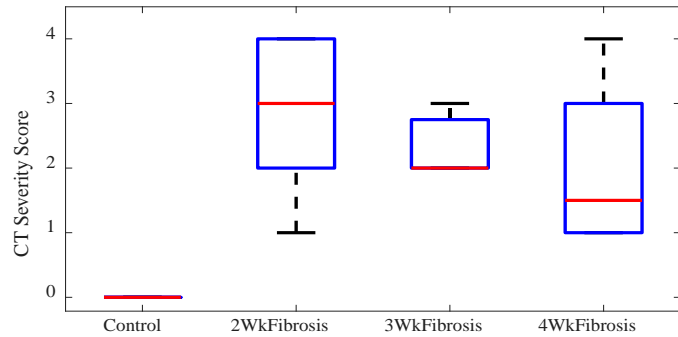


Figure 7: Severity scores based on bleomycin administration time (CT)

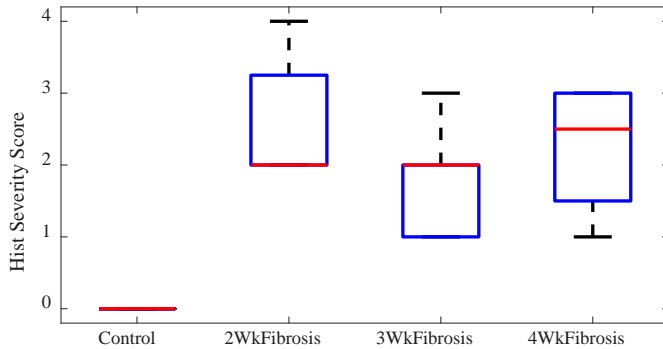


Figure 8: Severity scores based on bleomycin administration time (Histology)

We hypothesize that the bleomycin model is not a permanent model for inducing fibrosis in the rodents. The bleomycin rodent model hits its peak fibrosis at 2 weeks and eventually starts subsiding. The masked CT and histology severity scores were also compared to check if both methodologies quantified fibrosis in a similar manner.

Figure 9 shows that histology and CT scores were well aligned, and that both histologic severity and CT scan severity of pulmonary fibrosis, each scored categorically by a different masked observer, correlated well with SMFP assessed by ultrasound. The trend between the CT severity and histology severity score is a positive and significant one, with  $p < 0.001$ , strengthening the confidence in the results (Fig.9, left). The trend between the CT severity and SMFP values is a positive and significant one, with  $p < 0.05$  (Fig.9, Center). The trend between the histology severity score and SMFP values is a positive and significant one, with  $p < 0.005$  (Fig.9, right).

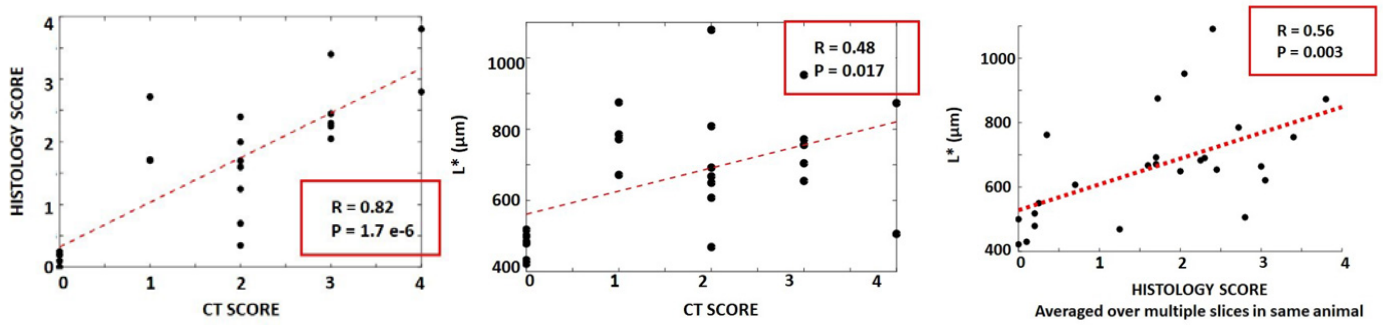


Figure 9. Left: CT ordinal score correlated with ordinal histology score. There are 6 scores matching at 0-0 (shams). Middle: Ordinal CT score correlated with SMFP ( $L^*$ ). Right: Ordinal histology score correlated with SMFP ( $L^*$ ).

As shown in figure 10, the BFS values were found to be  $-0.68 \pm 0.18$  MHz/cm,  $-0.39 \pm 0.12$  MHz/cm and  $-0.67 \pm 0.12$  MHz/cm for control, edematous and fibrotic lungs respectively. Significant difference were observed between BFS of control and edematous lungs ( $p < 0.001$ ) and between fibrotic and edematous lungs ( $p < 0.001$ ). No significant differences were observed between the BFS values of control and fibrotic lungs. We propose to combine the quantification of the SMFP and of the BFS in order to diagnose pulmonary fibrosis and pulmonary edema. A method involving those two parameters could be envisioned,

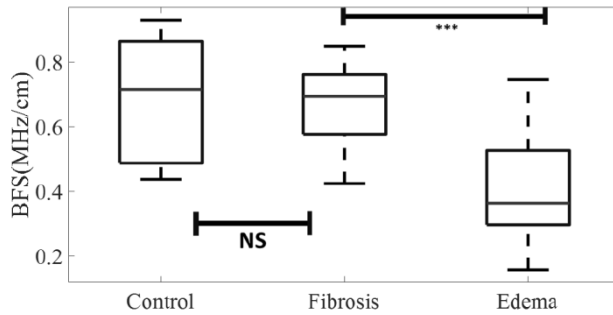


Figure 10: Distributions of BFS values for control ( $N=6$ ), edematous ( $N=6$ ) and fibrotic ( $N=6$ ) lungs. NS: non significant.

### 3.3 Opportunities for training

Kaustav Mohanty, a PhD student was trained and accomplished most of the experiments and data analysis. He graduated in 2019 and is now an engineer with GE healthcare.

### 3.4 Result dissemination

The results were presented at the meeting of the Acoustical Society of America in May 2019, as well as the International Ultrasound Symposium in October 2019. Some of the results were summarized in a technical article submitted to the Transactions in Ultrasonics Ferroelectrics and Frequency Control. The article is currently under review. We anticipate submitting a second journal article summarizing the results obtained during the next reporting period to a clinical journal in the future.

### **3.5 Objectives for the next reporting period**

Overall, these data support our hypothesis that measurement of SMFP is feasible and related to the severity of fibrosis. Additional experiments are warranted to provide a more controlled and wider range of severity of pulmonary fibrosis. We are currently using our no cost extension to create such a wider range of severity of pulmonary fibrosis, by instilling bleomycin and subsequently treating the animals with nintedanib. The study had to be halted due to the labs being closed due to the current pandemic, but was resumed last week.

## **4. Impact**

### **4.1 Impact on the development of the principal discipline of the project**

We successfully demonstrated that for a Sprague-Dawley rat lung, the transport mean free path was able to differentiate control from fibrosis. SMFP was obtained by separating the coherent and the incoherent backscattered intensities and calculating  $D$  which represented the dynamic growth of the diffusive halo. SMFP is a representation of how the wave diffuses in the lung parenchyma. In control lungs, due to the large amounts of air scatterers and large air volume, the growth of the diffusive halo is restricted leading to low SMFP values. On the contrary, in fibrotic rat lungs, the extensive thickening of the interlobular septa allowed for the wave to diffuse freely in lung parenchyma thereby accentuating the value of the diffusion constant  $D$  and SMFP.

There was a good correlation between SMFP and degree of fibrosis on CT scans, and the degree of fibrosis assessed by histology. Both assessments were (CT and histology) were done by independent experts who were not aware of the SMFP measurements. To ensure that each expert knew what a normal lung looked like, 3 control specimens were identified for each expert. The other 3 normal lungs were not identified, but were scored “0” by each expert. No fibrotic lung was assigned a score of zero by either expert. Our data implies that severity of fibrosis assessed radiographically and by histology was very similar.

We also demonstrated that the backscatter frequency shift was a relevant parameter to discriminate fibrotic from edematous lungs, which had similar values of SMFP.

This suggests the potential of ultrasound parameters related to multiple scattering and diffusivity to detect and stage lung pathologies such as pulmonary fibrosis, allowing monitoring response to treatment.

### **4.2 Impact on other disciplines**

We will investigate whether these methods can be used to follow COVID-19 patients.

### **4.3 Impact on technology transfer**

A provisional patent was filed in April 2020 (Appl. No. 63/014,092).

### **4.4 Impact on society beyond science and technology**

Nothing to report.

## 5. Changes/Problems

No changes to the proposed experimental approach were implemented.

No significant problems were encountered. Some minor challenges and learned phenomena are described here.

First the rat lungs are smaller than the probe, allowing information from the periphery of the lungs to creep in and over-predicting  $L^*$  values. This can be seen in the high standard deviations for  $L^*$ .

Second, it would be beneficial to trigger the ultrasound scanner with the rodent respirator to ensure that data is acquired perfectly at the end of the exhaling cycle to ensure maximum ultrasound penetration into the lung parenchyma.

We believe that in larger animal models, or in humans, combined with a more controlled experimental environment (acquisition at exhaling), these error bars can be reduced.

It was also noticed that after bleomycin treatment of the rats, fibrosis effects peaked at two weeks as predicted by CT, histology and  $L^*$  values. After two weeks, the severity of fibrosis started diminishing, or at the very least, stopped worsening. This is why we requested an extended period of performance, to perform a study in which pulmonary fibrosis will be induced, and rats will be treated with nintedanib.

Last, out of the 242 ultrasound data sets acquired, we were only able to extract trends with  $R^2 > 0.4$  69% of the times. The other 31% didn't exhibit trends that could allow the assessment of the transport mean free path (SMFP). This could be attributed to the fact that if the data was acquired at the peak inhaling stage, the reflection would be too strong and hence penetration would be lower than what is required for an incoherent trend to be visible. In humans, a 1 second breath hold at peak exhaling will be requested.

## 6. Products, Inventions, Patent Applications, and/or Licenses

A provisional patent was filed in April 2020 (Appl. No. 63/014,092).

A journal article was submitted to the Transactions in Ultrasonics Ferroelectrics and Frequency Control. The article is currently under review. We anticipate submitting a second journal article summarizing the results obtained during the next reporting period to a clinical journal in the future.

## 7. Participants & Other Collaborating Organizations

### **Thomas Egan, MD, MSc**

University of North Carolina at Chapel Hill

Dr. Egan (co Investigator) has developed and performed the rat model of fibrosis, and has supervised animal experiments.

### **Kaustav Mohanty, PhD**

North Carolina State University

Dr. Mohanty was a PhD student and was involved in all ultrasound experiments as well as ultrasound algorithm development and data analysis. He graduated in 2019.

## 8. Special Reporting Requirements

### Appendices

None

### References:

- Agricola, Eustachio, Tiziana Bove, Michele Oppizzi, Giovanni Marino, Alberto Zangrillo, Alberto Margonato, and Eugenio Picano. 2005. “‘Ultrasound Comet-Tail Images’: A Marker Of Pulmonary Edema.” *Chest*. doi:10.1378/chest.127.5.1690.
- Ashcroft, T., J. M. Simpson, and V. Timbrell. 1988. “Simple Method of Estimating Severity of Pulmonary Fibrosis on a Numerical Scale.” *Journal of Clinical Pathology* 41 (4): 467–70. doi:10.1136/jcp.41.4.467.
- Aubry, Alexandre, and Arnaud Derode. 2007. “Ultrasonic Imaging of Highly Scattering Media from Local Measurements of the Diffusion Constant: Separation of Coherent and Incoherent Intensities.” *Physical Review E - Statistical, Nonlinear, and Soft Matter Physics* 75 (2): 1–9. doi:10.1103/PhysRevE.75.026602.
- Aubry, Alexandre, Arnaud Derode, and Frederic Padilla. 2008. “Local Measurements of the Diffusion Constant in Multiple Scattering Media: Application to Human Trabecular Bone Imaging.” *The Journal of the Acoustical Society of America* 123 (5): 3633. doi:10.1121/1.2934875.
- Chaudhary, Nveed I., Andreas Schnapp, and John E. Park. 2006. “Pharmacologic Differentiation of Inflammation and Fibrosis in the Rat Bleomycin Model.” *American Journal of Respiratory and Critical Care Medicine*. doi:10.1164/rccm.200505-717OC.
- Crystal, Ronald G., Peter B. Bitterman, Brooke Mossman, Marvin I. Schwarz, Dean Sheppard, Laura Almsy, Harold A. Chapman, et al. 2002. “Future Research Directions in Idiopathic Pulmonary Fibrosis: Summary of a National Heart, Lung, and Blood Institute Working Group.” *American Journal of Respiratory and Critical Care Medicine* 166 (2): 236–46. doi:10.1164/rccm.2201069.
- Desai, Sujal R., Srihari Veeraraghavan, David M. Hansell, Ageliki Nikolakopoulou, Nicole S. L. Goh, Andrew G. Nicholson, Thomas V. Colby, et al. 2007. “CT Features of Lung Disease in Patients with

- Systemic Sclerosis: Comparison with Idiopathic Pulmonary Fibrosis and Nonspecific Interstitial Pneumonia.” *Radiology*. doi:10.1148/radiol.2322031223.
- Gargani, L., F. Frassi, G. Soldati, P. Tesorio, M. Gheorghiade, and E. Picano. 2008. “Ultrasound Lung Comets for the Differential Diagnosis of Acute Cardiogenic Dyspnoea: A Comparison with Natriuretic Peptides.” *European Journal of Heart Failure*. doi:10.1016/j.ejheart.2007.10.009.
- Gargani, Luna, Marica Doveri, Luigia D’Errico, Francesca Frassi, Maria L. Bazzichi, Andrea Delle Sedie, Maria C. Scali, et al. 2009. “Ultrasound Lung Comets in Systemic Sclerosis: A Chest Sonography Hallmark of Pulmonary Interstitial Fibrosis.” *Rheumatology (Oxford, England)*. doi:10.1093/rheumatology/kep263.
- Hübner, Ralf Harto, Wolfram Gitter, Nour Eddine El Mokhtari, Micaela Mathiak, Marcus Both, Hendrik Bolte, Sandra Freitag-Wolf, and Burkhard Bewig. 2008. “Standardized Quantification of Pulmonary Fibrosis in Histological Samples.” *BioTechniques* 44 (4): 507–17. doi:10.2144/000112729.
- Jambrik, Zoltan, Simonetta Monti, Vincenzo Coppola, Eustachio Agricola, Gaetano Mottola, Massimo Miniati, and Eugenio Picano. 2004. “Usefulness of Ultrasound Lung Comets as a Nonradiologic Sign of Extravascular Lung Water.” *American Journal of Cardiology*. doi:10.1016/j.amjcard.2004.02.012.
- Katzenstein, Anna-luise a, and Jeffrey L Myers. 1998. “Idiopathic Pulmonary Fibrosis Clinical Relevance of Pathologic Classification Clinical Features of the Idiopathic Interstitial Pneumonias.” *American Journal of Respiratory and Critical Care Medicine* 157: 1301–15. doi:10.1164/ajrccm.157.4.9707039.
- Launay, David, Martine Remy-Jardin, Ulrique Michon-Pasturel, Ioana Mastora, Eric Hachulla, Marc Lambert, Valerie Delannoy, et al. 2006. “High Resolution Computed Tomography in Fibrosing Alveolitis Associated with Systemic Sclerosis.” *Journal of Rheumatology*.
- Lichtenstein, Daniel A. 2016. *Lung Ultrasound in the Critically Ill. The BLUE Protocol*. doi:10.1007/978-3-319-15371-1.
- Moeller, Antje, Kjetil Ask, David Warburton, Jack Gauldie, and Martin Kolb. 2008. “The Bleomycin

- Animal Model: A Useful Tool to Investigate Treatment Options for Idiopathic Pulmonary Fibrosis?" *International Journal of Biochemistry and Cell Biology* 40 (3): 362–82.  
doi:10.1016/j.biocel.2007.08.011.
- Mohanty, Kaustav, John Blackwell, Thomas Egan, and Marie Muller. 2017. "Characterization of the Lung Parenchyma Using Ultrasound Multiple Scattering." *Ultrasound in Medicine & Biology* 43 (5): 993–1003. doi:10.1016/j.ultrasmedbio.2017.01.011.
- Picano, Eugenio, Francesca Frassi, Eustachio Agricola, Suzana Gligorova, Luna Gargani, and Gaetano Mottola. 2006. "Ultrasound Lung Comets: A Clinically Useful Sign of Extravascular Lung Water." *Journal of the American Society of Echocardiography*. doi:10.1016/j.echo.2005.05.019.
- Reißig, Angelika, and Claus Kroegel. 2003. "Transthoracic Sonography of Diffuse Parenchymal Lung Disease: The Role of Comet Tail Artifacts." *Journal of Ultrasound in Medicine*.  
doi:10.7863/jum.2003.22.2.173.
- Robbe, Alexandre, Alexandra Tassin, Justine Carpentier, Anne Emilie Declèves, Zita Léa Mekinda Ngono, Denis Nonclercq, and Alexandre Legrand. 2015. "Intratracheal Bleomycin Aerosolization: The Best Route of Administration for a Scalable and Homogeneous Pulmonary Fibrosis Rat Model?" *BioMed Research International* 2015: 1–10. doi:10.1155/2015/198418.
- Rojas, Mauricio, Jianguo Xu, Charles R. Woods, Ana L. Mora, Willy Spears, Jesse Roman, and Kenneth L. Brigham. 2005. "Bone Marrow-Derived Mesenchymal Stem Cells in Repair of the Injured Lung." *American Journal of Respiratory Cell and Molecular Biology*. doi:10.1165/rcmb.2004-0330OC.
- Sayed, SuzanS, GamalM Agmy, AzzaF Said, and AhmedH Kasem. 2016. "Assessment of Transthoracic Sonography in Patients with Interstitial Lung Diseases." *Egyptian Journal of Bronchology* 10 (2): 105. doi:10.4103/1687-8426.184375.
- Soldati, G., and S. Sher. 2009. "Bedside Lung Ultrasound in Critical Care Practice." *Minerva Anestesiologica* 75 (9): 509–17. doi:10.1186/cc5668.
- Tourin, Arnaud, Arnaud Derode, Aymeric Peyre, and Mathias Fink. 2000. "Transport Parameters for an Ultrasonic Pulsed Wave Propagating in a Multiple Scattering Medium." *The Journal of the*

*Acoustical Society of America* 108 (2): 503. doi:10.1121/1.429580.

Volpicelli, Giovanni, Alessandro Mussa, Giorgio Garofalo, Luciano Cardinale, Giovanna Casoli, Fabio Perotto, Cesare Fava, and Mauro Frascisco. 2006. "Bedside Lung Ultrasound in the Assessment of Alveolar-Interstitial Syndrome." *American Journal of Emergency Medicine* 24 (6): 689–96. doi:10.1016/j.ajem.2006.02.013.

Xu, Jianguo, Ana L. Mora, John LaVoy, Kenneth L. Brigham, and Mauricio Rojas. 2006. "Increased Bleomycin-Induced Lung Injury in Mice Deficient in the Transcription Factor T-Bet." *American Journal of Physiology-Lung Cellular and Molecular Physiology*. doi:10.1152/ajplung.00006.2006.

Yang, Feng, Wee Ser, Jufeng Yu, David Chee-Guan Foo, Daniel Poh Shuan Yeo, Pow-Li Chia, and Jennifer Wong. 2012. "Lung Water Detection Using Acoustic Techniques." *Conference Proceedings : ... Annual International Conference of the IEEE Engineering in Medicine and Biology Society. IEEE Engineering in Medicine and Biology Society. Annual Conference 2012*: 4258–61. doi:10.1109/EMBC.2012.6346907.